Identification of Plasma Membrane Macro- and Microdomains from Wavelet Analysis of FRET Microscopy

Evgeny Kobrinsky,* Donald E. Mager,* Sarah A. Bentil,* Shin-ichi Murata,† Darrell R. Abernethy,* and Nikolai M. Soldatov*

*National Institute on Aging, National Institutes of Health, Baltimore, Maryland; and †Department of Pathology, Interdisciplinary Graduate School of Medicine and Engineering, University of Yamanashi, Yamanashi, Japan

ABSTRACT In this study, we sought to characterize functional signaling domains by applying the multiresolution properties of the continuous wavelet transform to fluorescence resonance energy transfer (FRET) microscopic images of plasma membranes. A genetically encoded FRET reporter of protein kinase C (PKC)-dependent phosphorylation was expressed in COS1 cells. Differences between wavelet coefficient matrices revealed several heterogeneous domains (typically ranging from 1 to 5 μm), reflecting the dynamic balance between PKC and phosphatase activity during stimulation with phorbol-12,13-dibutyrate or acetylcholine. The balance in these domains was not necessarily reflected in the overall plasma membrane changes, and observed heterogeneity was absent when cells were exposed to a phosphatase or PKC inhibitor. Prolonged exposure to phorbol-12,13-dibutyrate and acetylcholine yielded more homogeneous FRET distribution in plasma membranes. The proposed wavelet-based image analysis provides, for the first time, a basis and a means of detecting and quantifying dynamic changes in functional signaling domains, and may find broader application in studying fine aspects of cellular signaling by various imaging reporters.

INTRODUCTION

The heterogeneity of biological signaling events forms the basis for conceptualizing the plasma membrane of cells as an array of microdomains of signaling molecules (Maxfield, 2002; Vermeer et al., 2004). Owing to advances in live cell imaging, it has become possible to monitor the activity of a variety of signaling molecules in live cells. Fluorescence resonance energy transfer (FRET) microscopy is a popular tool for revealing the interaction of signaling molecules, highlighting nanometer-scale associations in cellular milieu (Wallrabe et al., 2003; Kobrinsky et al., 2004; Sharma et al., 2004). FRET essentially involves the transfer of energy from an excited donor fluorophore to an acceptor fluorophore, providing that the two fluorophores are within a certain proximity (1–10 nm). Thus, FRET microscopy is often regarded as a *molecular ruler*, which forms the rationale for its use in imaging molecular interactions (Kenworthy, 2001). Additionally, FRET microscopy can be used for the detection of conformational changes in reporter molecules, where fluorescent groups are attached to the same molecule. Rearrangements of the fluorophores, induced by activation of opposing processes (e.g., phosphorylation/dephosphorylation), are then detected by FRET microscopy and thereby represent the dynamic activity of a functional signaling domain. Analysis of signaling in the plasma membrane presents certain challenges reflecting a dynamic process taking place in a confined space. Numerous studies aimed at the plasma membrane have provided indirect evidence for the existence of distinct signaling domains. However, despite an increasing interest in plasma membrane signaling, the image analysis of the formation and function of signaling domains is not yet completely developed. In this work, we propose a wavelet-based image analysis to detect and quantify dynamic changes in functional signaling domains with an example of the protein kinase C (PKC) activity in plasma membranes of live cells. The PKC signaling cascade is important for various cell functions (Shirai and Saito, 2002), and phosphorylation of plasma membrane proteins represents a key step in cell signaling. We expressed the C kinase activity reporter (CKAR) of PKC phosphorylation activity (Violin et al., 2003) confined to the plasma membrane, offering a method for detecting phosphorylation/dephosphorylation activity of protein kinase C and phosphatase in such an environment. We utilized this system as a model for developing a wavelet-based approach for FRET microscopy, allowing for the detection of macro- and microfunctional signaling domains.

Our overall approach is illustrated in Fig. 1, which begins with a narrowing-down of manually outlined regions of interest (ROI_m) defined as the plasma membrane region with obvious signals of fluorescence and little or no interference from fluorescence of other cellular compartments (Fig. 1 *A*, *left panel*). Our aim is to narrow-down ROI_m using statistical comparisons of FRET matrices and to identify domains of signaling within the statistically redefined ROI_s (Fig. 1 *A*, *right panel*). FRET values within the redefined ROI_s are linearized over the plasma membrane perimeter transforming

Submitted October 5, 2004, and accepted for publication February 11, 2005.

Evgeny Kobrinsky and Donald E. Mager contributed equally to this work.

Address reprint requests to Nikolai M. Soldatov, Tel.: 410-558-8343; E-mail: soldatovn@grc.nia.nih.gov.

Donald E. Mager's present address is Dept. of Pharmaceutical Sciences, University at Buffalo, State University of New York, Buffalo, NY.

0006-3495/05/05/3625/10 $2.00

doi: 10.1529/biophysj.104.054056

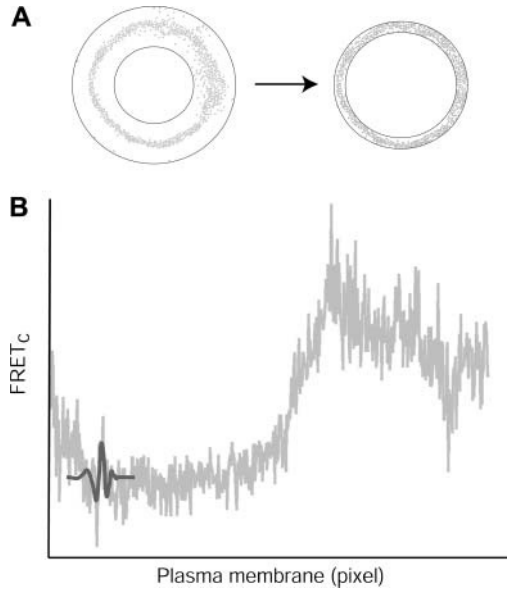

FIGURE 1 Schematic of wavelet analysis of FRET microscopy. (*A*) ROI_m (*left panel*, two *solid circles*) localizing clear instances of FRET signal (*shaded dots*) are then narrowed-down (*right panel*) by statistically comparing, pixel-by-pixel, control and stabilized images where maximum changes in FRET signal have been observed. (*B*) Corrected FRET values in redefined ROI (*A*, *right*) are transformed into linearized one-dimensional signals for texture and wavelet analysis. Wavelet analysis involves comparing a scaled wavelet basis function (db4 wavelet is shown in *solid representation*) to the signal, an amplitude coefficient is calculated, and then the wavelet is shifted along the *x* axis (space) and continues across the duration of the signal. The wavelet is then rescaled (corresponding to new frequency) and the process is repeated. This procedure results in a matrix of wavelet coefficients that co-localize in space and frequency and is summarized by Eq. 7.

two-dimensional images of the plasma membrane into one-dimensional signals (Fig. 1 *B*). These signals are subjected to a continuous wavelet transform and temporal differences between wavelet coefficient matrices are used to identify heterogeneous domains. FRET intensity in identified domains can then be compared over time to ascertain their dynamics and potential for representing functional signaling domains. The spatial resolution of this method is limited by the diffraction limit of 250 nm (the pixel size in our experiments). This method provides a means of elucidating the spatial heterogeneity in the dynamics of phosphorylation/dephosphorylation of PKC substrates in the plasma membrane and may be extended to a wide variety of recently developed FRET-based indicators (Zaccolo, 2004).

MATERIALS AND METHODS

Materials

The CKAR-pcDNA3 was kindly provided by Drs. R.Y. Tsien and A.C. Newton (University of California, San Diego, CA). The PKC activator phorbol-12,13-dibutyrate (PDBu), a specific PKC inhibitor (Gö6983), and a cell-permeable phosphatase inhibitor (calyculin A) were purchased from Calbiochem (La Jolla, CA). All other chemicals were obtained from Sigma (St. Louis, MO).

Cell culture and transfection

COS1 cells were grown on poly-D-lysine-coated coverslips (MatTek, Ashland, MA) in DMEM supplemented with 10% fetal calf serum. COS1 cells were transfected with CKAR-pcDNA3 using the Effectene kit (Qiagen, Valencia, CA).

FRET imaging and image analysis

Images were recorded in live transfected COS1 cells with a Hamamatsu digital camera C4742-95 mounted on the Nikon epifluorescent microscope TE200 (60 × 1.2 N.A. objective) equipped with multiple filter sets (Chroma Technology, Rockingham, VT). Excitation light was provided by a 175 W Xenon lamp. C-Imaging (Compix, Cranberry Township, PA) and MetaMorph (Universal Imaging) software were used to obtain and analyze FRET images. FRET was quantified with the following three filter sets: for the acceptor monomeric yellow fluorescent protein (YFP) cube, excitation filter 500/20 nm, dichroic beam splitter 515 nm, emission filter 535/30 nm; for the donor monomeric cyan fluorescent protein (CFP) cube, excitation filer 436/20 nm, dichroic beam splitter 455 nm, emission filter 480/30 nm; and for the FRET (CFP/YFP) cube, excitation 436/20 nm, dichroic beam splitter 455 nm, emission filter 535/40 nm. Excitation filter sets were changed by a high-speed filter wheel system (Lambda 10-2, Sutter Instruments, Novato, CA). The simultaneous acquisition of two fluorescence images (donor and FRET) was achieved with the Dual-View system (Optical Insights, LLC, Santa Fe, NM), which was attached to the microscope. The time of acquisition varied from 50 to 300 ms, but was held constant during a given experiment. ROI_m was selected from the plasma membrane of a control cell, where there were obvious signals of fluorescence and little or no interference from fluorescence from the intracellular compartment. ROI_m was selected using the C-Imaging software program, where intensity (*I*) from three filter sets was determined after background subtraction. FRET values were calculated in each pixel and averaged across the ROI_m (with one ROI_m per cell). The full scale of digitized resolution ranged from 0 to 255. Corrected intensity of FRET ($FRET_c$) was calculated as

$$FRET_c = I_{FRET} - I_{CFP} \times A - I_{YFP} \times B, \quad (1)$$

where bleedthrough coefficients ($A = 0.73$ and $B = 0.08$) were determined experimentally by calibration according to Xia and Liu (2001). This calibration is based on the measurements of fluorescence of the CFP- and YFP-labeled constructs expressed in COS1 cells in all three filter sets to determine bleedthrough in CFP, YFP, and FRET filters (for additional details, see Kobrinsky et al., 2003). Corrected FRET values were normalized by donor and acceptor levels, $FRET_N = FRET_C/(I_{CFP} \times I_{YFP})^{1/2}$, according to Xia and Liu (2001). Experiments resulting in images with pixel shifts were discarded and only experiments with no pixel shifts were analyzed.

Redefining the plasma membrane region

For pixel-by-pixel calculations, three consecutive images of one and the same cell before ACh or PDBu exposure (control images), along with three consecutive images after prolonged PKC activation when stabilized effect (SE) was reached (at 5 min for ACh and 15 min for PDBu), were converted, by importation to Excel (MicroSoft, Redmond, WA), into a spreadsheet view in a matrix format. ROI_m of the control cell image (see above) was superimposed onto all $FRET_c$ matrices, and fluorescence values outside the ROI_m were zeroed. Then the paired *t*-test was applied to each pixel comparing mean values between the control and SE images. Timepoints to be compared with control images (5 min for ACh and 15 min for PDBu)

were selected based on stabilization of changes in FRET signals. For example, average FRET over ROI was found to be decreased to approximately the same extent as FRET in images sampled at 14- and 16-min (see Fig. 2 *B*, *inset*). This corresponds to the time required for stabilization of the PDBu application (10–15 min) reported by Violin et al. (2003). Statistical difference between the means of each pixel was determined, and the ROI were narrowed down to only those pixels exhibiting a statistically significant difference ($p < 0.05$). Any gaps were filled by including statistically nonsignificant pixels to connect these regions (up to 3 pixels thick), redefining a continuous plasma membrane region. For subsequent analyses, final matrices were linearized or transformed into one-dimensional signals using a simple algorithm (see Supplementary Material) in MatLab (The MathWorks, Natick, MA).

Texture analysis

Texture analysis of FRET microscopy includes global assessments of image properties. Analysis of the redefined ROI_s was performed according to Murata et al. (2001; 2003). The values of angular second momentum (ASM), sum of variance (SVar), and difference variance (DVar) were calculated from normalized gray-tone (8-bit) spatial-dependence matrices (co-occurrence matrices per Haralick et al., 1973), reflecting spatial homogeneity, spatial heterogeneity, and contrast, respectively, according to

$$ASM = \sum_{i=1}^{Ng}\sum_{j=1}^{Ng}\{P(i,j)\}^2 \tag{2}$$

$$SVar = \sum_{k=2}^{2Ng}\left(k - \sum_{k=2}^{2Ng} k \cdot P_{x+y}(k)\right)^2 \times P_{x+y}(k) \tag{3}$$

$$DVar = \sum_{k=0}^{Ng}\left(k - \sum_{k=0}^{Ng} k \cdot P_{x-y}(k)\right)^2 \times P_{x-y}(k), \tag{4}$$

where $P_{x+y}(k)$ and $P_{x-y}(k)$ are from (Haralick et al., 1973)

$$P_{x+y}(k) = \sum_{i=1}^{Ng}\sum_{j=1}^{Ng} P(i,j) \quad k = 2, 3, \ldots, 2Ng \tag{5}$$

$$P_{x-y}(k) = \sum_{i=1}^{Ng}\sum_{j=1}^{Ng} P(i,j) \quad k = 0, 1, \ldots, Ng - 1. \tag{6}$$

The term $P(i,j)$ is the $(i,j)^{th}$ entry in a co-occurrence matrix, and Ng is the number of distinct gray levels in the image. For illustration with the PKC model, these calculations were made for control and 5- (ACh) or 15-min (PDBu) images.

Wavelet analysis

The continuous wavelet transform (CWT) of a linearized spatial signal $f(x)$ (amplitude over distance) is defined as

$$C_{ab} = \int_{-\infty}^{\infty} f(x)\frac{1}{(|a|)^{1/2}}\Psi * [(x-b)/a]dx, \tag{7}$$

where a represents scale, b is the translation parameter (shift in space), and Ψ represents the wavelet basis function. Calculated coefficients (C_{ab}) of the wavelet transform reflect an amplitude or the correlation between the original signal and the basis function at different scales and positions in space. The scale parameter is inversely related to frequency. Thus large-scale values allow for the global analysis of the low-frequency components of the spatial signal, whereas small scales provide a means for local analysis of the high-frequency components. For more details, Aristizabal and Glavinovic (2003) provide an excellent introduction to the fundamentals of wavelet analysis.

There are several families of wavelets and the choice of a wavelet basis function is often made arbitrarily or via a trial-and-error check. Unlike some wavelets that are infinite and defined by analytic formulas, Daubechies (db) wavelets are the limits of an iterative process and have the value zero everywhere outside a specific interval or support. Thus, in addition to other mathematical properties, db wavelets have compact support and can be used in local analysis (Misiti et al., 2000). For comparison purposes, a CWT with db4, db9, and the Haar wavelet basis functions was applied to each signal of linearized FRET values in the statistically defined ROI. The numbers associated with the db wavelets correspond to the order of the wavelet and the Haar wavelet is the simplest basis function, resembling a step function. The number of examined scales ranged from 32 to 96, depending on the length of a given signal, but was held constant for each cell. Temporal differences (D) in wavelet coefficient matrices (C) were assessed by computing the squares of the differences $D_t = (C_C - C_t)^2$, where the subscripts C and t represent control and time. Difference coefficient matrices were normalized by the maximal square difference and rendered in two-dimensional pseudo-color maps as a function of scale and space. Domains were identified initially by visual inspection of areas of ''hot'' color, which indicate a change in signal heterogeneity. Each initial domain was then scrutinized using a one-way ANOVA with Dunnett's multiple comparisons test, where the mean and standard deviation of $FRET_c$ values within a domain were compared at the zero, 1-min, and SE timepoints. Only those domains that showed statistically significant temporal changes in FRETc values were finally selected as signaling domains of interest. Standard deviations of wavelet coefficients were calculated also at each scale, providing an objective measure of coefficient dispersion that could be monitored over time. All calculations associated with wavelet analysis were performed using MatLab.

RESULTS

FRET was used in our experiments to detect PKC-mediated phosphorylation in the plasma membrane of COS1 cells expressing CKAR as a reversible phosphorylation reporter. CKAR is composed of monomeric CFP, monomeric YFP, and a PKC substrate peptide tethered by a flexible linker to an FHA2 phosphothreonine-binding domain. The 10 amino-terminal residues of Lyn kinase that contain signals for myristoylation and palmitoylation were fused to CKAR to achieve targeting of the reporter to the plasma membrane. Phosphorylation of the PKC substrate results in its binding to the FHA2 domain, and a subsequent conformational change results in a decrease of the FRET signal between the CFP and YFP fluorophores, reversible by phosphatases (Violin et al., 2003). A decrease in FRET reflects an increase of PKC-mediated phosphorylation, whereas an increase in FRET corresponds to an increase in phosphatase activity. CFP and YFP fluorophores contained mutation A206K to reduce homoaffinity of all GFPs and preclude nonspecific clustering and intermolecular FRET by CFP-YFP dimerization (Zacharias et al., 2002).

Exposure to the PKC-activator phorbol dibutyrate (PDBu) produced changes in FRET signals, allowing for the real-time imaging of PKC-activation. An example of the PDBu effect on CKAR phosphorylation expressed in COS1 cells is shown in Fig. 2 *A*. It was essential to define the plasma membrane region that was the source of the FRET signal. To this end, we redefined the selected ROI_m (*middle panel*)

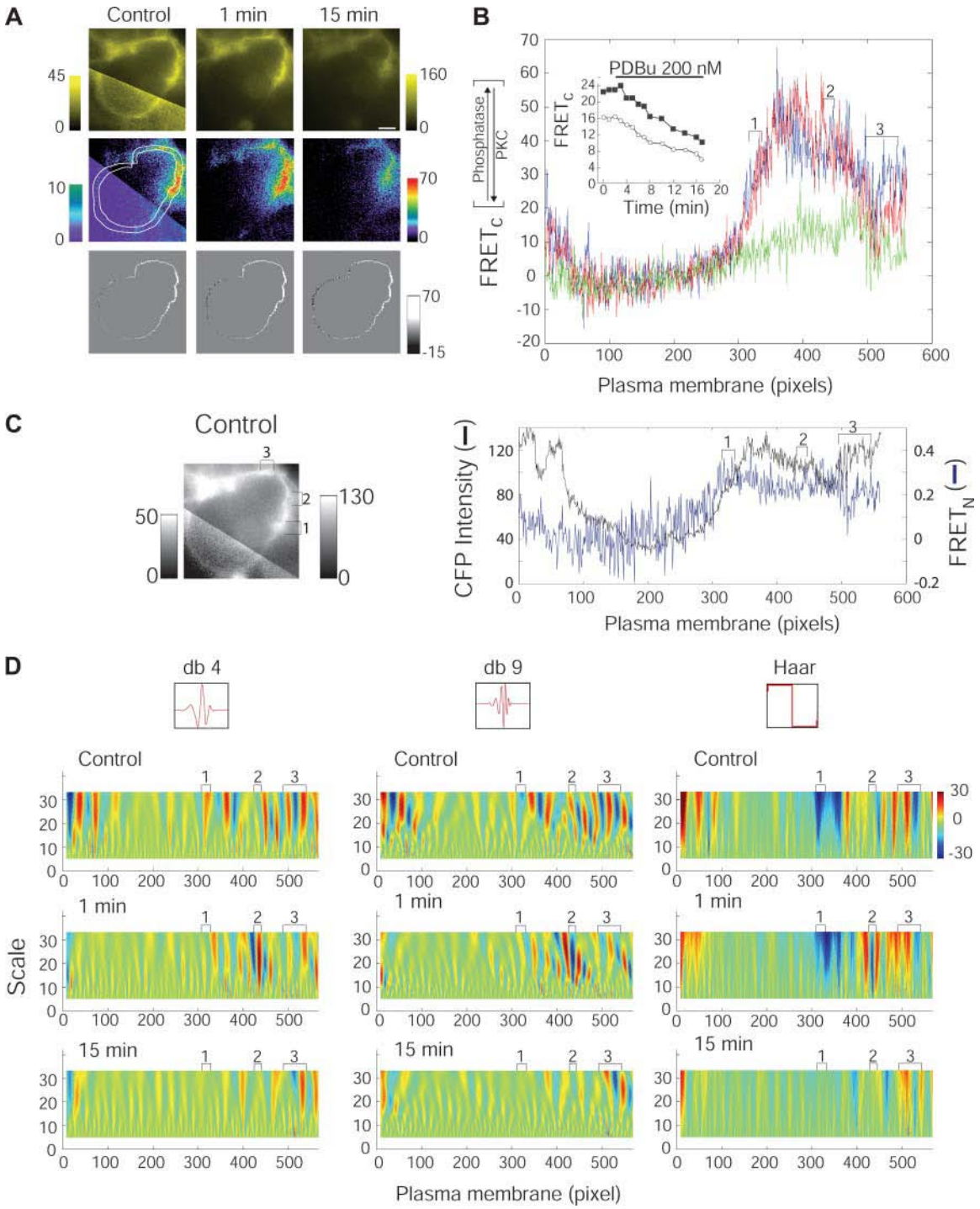

FIGURE 2 Wavelet analysis of PDBu-induced PKC activation in COS1 cells expressing the CKAR . (*A*) Progression from original FRET images to $FRET_c$ images within redefined plasma membrane ROI_s. FRET images of a COS1 cell obtained before (control) and after 1 (transient increase in FRET) or 15 min (stable decrease of FRET) of application of 200 nM PDBu (*top panels*), and corresponding $FRET_c$ images (*middle panels*, *white lines* show ROI_m), and shaded images of $FRET_c$ within redefined plasma membrane ROI_s (*bottom panels*). The top control image is shown in two different intensity scales to illustrate the cell plasma membrane continuity (*left scale* applies to the bottom part of the image). Scale bar is 3 μm. (*B*) $FRET_c$ values in the linearized plasma membrane ROI_s in control before (*blue*), and after 1 min (*red*) and 15 min (*green*) of PDBu application. (*Inset*) The time-dependence of $FRET_c$ values averaged over the plasma membrane ROI after activation of PKC in the manually (*open circles*) and statistically defined (*solid squares*) plasma membrane region. Both time-dependencies indicate a transient increase of CKAR FRET (1 min) followed by a continuous decrease of the $FRET_c$ signal. Decrease in $FRET_c$ was due to phosphorylation of the substrate part of CKAR by PKC. Brackets show db4 statistically defined signaling microdomains (see below). (*C*) Image of a CKAR-expressing COS1 cell obtained under control conditions with the CFP filter (*left*). Plasma membrane intensity profile obtained with the CFP filter, representing the spatial heterogeneity in the CKAR expression level (*solid line*), and FRET normalized by the level of expression ($FRET_N$, *blue line*) are shown on the right.

based on a statistical analysis (*lower panel*). The number of the statistically significant pixels was ~40% of the pixels in the ROI_m. Corrected FRET values in the redefined plasma membrane ROI_s were greater than those in the ROI_m, but followed a similar trend (Fig.2 *B*, *inset*). These plasma membrane regions were subsequently linearized for texture and wavelet analysis (Fig. 2 *B*). Fig. 2 *C* (*left panel*) shows the same image of a CKAR-expressing COS1 cell obtained with CFP filter before application of PDBu. The CFP (donor) intensity profile along the plasma membrane (Fig. 2 *C*, *right panel*) represents the level of CKAR expression. One can see that the CKAR expression is not homogeneous along the plasma membrane. FRET values normalized by the level of expression ($FRET_N$) are also plotted in Fig. 2 *C* (*right panel*). These values represent a balance between phosphorylation/dephosphorylation of CKAR and were not always correlated with the level of CKAR expression (compare $FRET_N$ and CFP intensity in Fig. 2 *C*, *right panel*). A high level of CKAR expression is observed in the left portion of Fig. 2 *C*, *right panel*, representing 0–100 pixels of the linearized plasma membrane. However, it corresponds to a low level of FRET signal in the respective region in Fig. 2 *B*, and $FRET_N$ in Fig. 2 *C*, *right panel*, indicating a low level of phosphatase activity or a high level of PKC activity in this part of the plasma membrane. The heterogeneity in the distribution of FRET levels along the plasma membrane under control conditions was produced by the heterogeneity of both CKAR expression and the balance of PKC-mediated phosphorylation/phosphatase activity. Our goal was to identify functional signaling domains based on temporal changes in the FRET signal along the plasma membrane that are not affected by heterogeneity of CKAR expression. The difference in expression levels is most likely produced by much slower processes than the time frame of changes we observed in the CKAR signal induced by PKC activation (Violin et al, 2003). Therefore, the identification of functional signaling domains was based on fast temporal changes (seconds and minutes) in FRET signaling, where the FRET-based CKAR reporter expression in each particular pixel of the obtained images is likely to be similar or relatively constant.

We applied a continuous wavelet transform (CWT) to the linearized membrane corrected FRET values at selected timepoints of PDBu application using, for comparison, the db4, db9, and Haar wavelet basis functions (Fig. 2 *D*). COS1 cells showed episodes of transient heterogeneity in the distribution of corrected FRET at high and low scale frequencies. After prolonged PDBu exposure, the distribution of the corrected FRET and wavelet coefficients along the plasma membrane became more homogeneous (Fig. 2 *D*). Texture analysis (Murata et al., 2001; 2003) revealed that the homogeneity of the corrected FRET values over the plasma membrane increased twofold after 15 min of PDBu application. Comparing the texture analysis parameters for the control and 15-min PDBu application data, we found that the *ASM* parameter (homogeneity) increased from 0.0011 to 0.0025, *SVar* (heterogeneity) decreased from 24,600 to 13,000, and *DVar* (contrast) decreased from 1330 to 625. The temporal heterogeneity of the corrected FRET distribution was observed in plots of the squares of differences in wavelet coefficients in the space-frequency domain (Fig. 3). These wavelet coefficient plots provided means of identifying domains at different spatial frequencies (see *brackets* in Fig. 2, *B–D*). A one-way ANOVA with Dunnett's multiple comparisons test was applied for 0, 1, and 15-min timepoints and statistically significant domains were selected. One of the important findings was that FRET changes in identified microdomains did not always correspond to the overall mean changes along the plasma membrane (Table 1). The size of the signaling domains was variable (see regions marked by *brackets* 1–3 in Fig. 2, *B–D*). Although obvious polarized changes in FRET in one part of the plasma membrane can define a macrodomain (Fig. 2 *B*), the sizes of microdomains typically did not exceed a few pixels, ranging from 1 to 5 μm. Similar domains of interest were identified with all three tested wavelet basis functions (Fig. 2 *D*). No significant changes in the structure of the domains were found for cells incubated with control solution at 5- and 15-min intervals (data not shown). Identification of functional signaling microdomains based on temporal changes of FRET values along the plasma membrane was not dependent on the difference in the level of CKAR expression, as can be seen from Fig. 2 *B* ($FRET_c$) and Fig. 2 *C* (CKAR expression level), where signaling microdomains (marked by *brackets* 1–3) are localized in a plasma membrane region with a relatively high and stable level of CKAR expression.

In a set of control experiments, COS1 cells were exposed to PDBu in the presence of a phosphatase inhibitor calyculin A. The transient increase in FRET values (normalized to control) observed after 1 min of PDBu exposure was absent in the calyculin A-treated cells (Fig. 4 *A*). Linearized corrected FRET ($FRET_c$, see Materials and Methods) values in the redefined ROI_s for a representative cell (Fig. 4 *B*, *left panel*) show that FRET intensities were relatively homogeneous even in the control image. The wavelet coefficients resulting from a CWT (db4) of the signals in Fig. 4 *B*, *left panel* are shown in Fig. 4 *C*, *left panel*, along with the

FIGURE 2 (Continued).

(*D*) Comparison of wavelet coefficients from a CWT analysis (values represented according to *color bar*) using db4, db9, and Haar wavelets at different timepoints (0, 1, and 15 min) of PDBu application in linearized plasma membrane (in pixels). At scale (see *y* axis) 5, the standard deviations of the coefficients were 5.02, 5.37, and 4.15 in control, 1-, and 15-min PDBu application for db4, respectively. Likewise at scale 32 (db4), the corresponding standard deviations were 11.1, 7.09, and 6.40. Scale (*y* axis) theoretically reflects the sampling period of the signal and is represented without reference to units. Domains defined by one-way ANOVA with Dunnett's multiple comparisons test are shown with brackets and correspond to those in *B*.

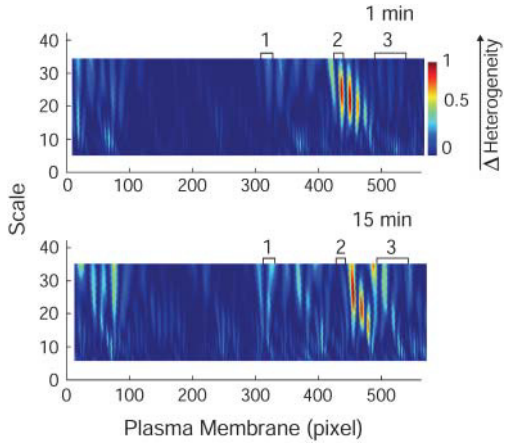

FIGURE 3 Subtraction of wavelet coefficient matrices as a tool for highlighting the heterogeneity of the plasma membrane domains. Subtraction of the 1-min (*top panel*) and 15-min timepoint (*bottom panel*) wavelet coefficient matrices from the control matrix, where the original matrices are shown in Fig. 2 *D* (db4). Subtraction of each matrix coefficient was done according to $D_t = (C_C - C_t)^2$, where D is the difference between the wavelet coefficient matrices at different timepoints (t), C_C is the coefficient matrix under control conditions, and C_t is the coefficient matrix after timepoints of PDBU action. D_t was normalized to the maximal value (see *color bar*).

domains of interest (bracketed) that were identified by examining the squared differences between wavelet coefficients at 1- and 15-min timepoints with control. Only in one of these domains was $FRET_c$ significantly decreased from control values after a 1-min PDBu and calyculin A exposure, whereas all domains showed significantly lower FRET intensity after 15 min. In agreement with the results obtained by averaging $FRET_c$ over the plasma membrane in Fig. 4 *A*, no single domain revealed an increase in $FRET_c$. Preincubation of cells with a specific PKC inhibitor (Gö6983) also resulted in a complete loss of the PDBu-induced transient increase in FRET. Additionally, 15-min application of Gö6983 eliminated the PDBu-induced decrease in FRET in accordance with the inhibition of PKC-mediated phosphorylation of the CKAR reporter (Fig. 4 *A*). Only one domain over entire plasma membrane ROI_m showed significant changes after 15 min of PDBu application (Fig. 4 *C*, *right panel*).

TABLE 1 Temporal changes in $FRET_c$ within identified microdomains

	Control versus 1 min		Control versus stabilized state*	
Domain†	Mean difference	*p*-value	Mean difference	*p*-value
PDBu				
1	6.216	<0.01	17.46	<0.01
2	−8.147	<0.01	21.78	<0.01
3	9.356	<0.01	18.86	<0.01
ACh				
1	−2.600	<0.05	−1.146	>0.05
2	−0.6123	>0.05	7.701	<0.01
3	2.445	>0.05	12.46	<0.01
4	8.188	<0.01	12.11	<0.01

*Domain numbers correspond to brackets in Figs. 2 and 5 for PDBu and ACh, respectively.
†Timepoints for stabilized effects for PDBu and ACh are 15 and 5 min, respectively.

Another example of the CWT application was based on stimulation of G protein-coupled receptors that can induce activation of PKC (Violin et al., 2003). We expressed the human M1 muscarinic type 1 receptor along with the CKAR construct in COS1 cells. Application of acetylcholine (ACh; 10 μM) induced a transient increase in FRET signal followed by a continuous decline (Fig. 5 *A*, *inset*). Similar to the PDBu treatment, wavelet analysis of the linearized $FRET_c$ image (Fig. 5 *A*) revealed membrane microdomains (marked by *brackets* 1–4) that responded to 1-min ACh application differently from the overall plasma membrane $FRET_c$ plotted in the *inset* (Fig. 5 *A*). For example, the overall FRET signal at the 1-min timepoint was slightly increased (Fig. 5 *A*), as was $FRET_c$ in microdomain 1, whereas microdomains 3 and 4 showed a decrease in FRET signal (Table 1). This may suggest that the phosphorylation/dephosphorylation status of the CKAR reporter was not uniform over the plasma membrane. With the exception of *ASM*, parameters of the texture analysis of the ACh-stimulated PKC phosphorylation followed a similar trend as the PDBu exposure, where *ASM* decreased from 0.0043 to 0.0009, *SVar* decreased from 54,100 to 10,500, and *DVar* decreased from 5570 to 1320. Overall, there is general agreement between the wavelet and texture analyses, whereby both methods suggest a decrease in the heterogeneity of corrected FRET values after extended (5 min) PKC activation by ACh.

A three-dimensional representation of $FRET_c$ and identified signaling domains in ROI_s for both PDBu- and ACh-treated cells (Fig. 6; note that regions outside the ROI_s were zeroed as described previously) revealed the spatial localization and temporal characteristics of identified domains. For example, the $FRET_c$ intensity in domain 2 for the PDBu-treated cell (previously identified in Fig. 2) is shown to increase at 1 min and decrease after 15 min of PDBu application (Fig. 6 *A*). This is in contrast to domains 1 and 3 that show decreasing $FRET_c$ at both the 1- and 15-min timepoints. A similar heterogeneity (Fig. 6 *B*) was revealed for the COS1 cell exposed to ACh (Fig. 5), where domain 1 shows a significant increase in FRET at 1 min, while domain 4 exhibits a significant decrease (Fig. 6 *B*). On the other hand, domains 2–4 all reveal significantly decreased $FRET_c$ after 5 min of ACh exposure.

DISCUSSION

Here we present a new method of identifying functional signaling domains in cellular plasma membranes based on a wavelet analysis of FRET imagining data. Such analyses require a continuous signal. If such a clear signal is present,

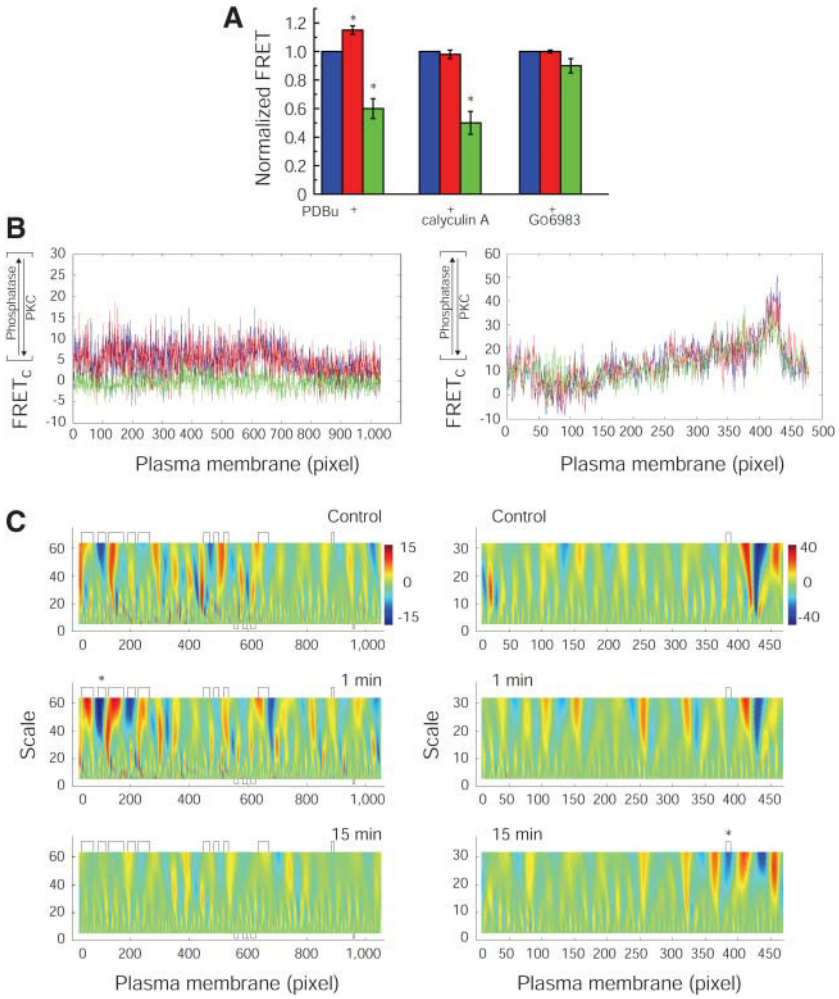

FIGURE 4 Transient phosphatase activation is sensitive to a phosphatase and PKC inhibitors, but the sustained PKC-induced phosphorylation is sensitive to only the PKC inhibitor. (*A*) Bar histogram showing the PDBu effect on normalized FRET values of CKAR reporter in the absence or in the presence of the inhibitors of phosphatase (calyculin A, 100 nM) or PKC (Gö6983, 1 μM). Colors correspond to control (*blue*) and 1- (*red*) and 15-min (*green*) timepoints of PDBu (200 nM) exposure. Normalized FRET increased to 1.15 $\pm$ 0.03 ($p < 0.05$; $n = 3$) after 1 min of PDBu action. Incubation with calyculin A and Gö6983 abolished this transient increase to 0.98 $\pm$ 0.03 ($n = 5$) and 1.00 $\pm$ 0.01 ($n = 3$), respectively. After prolonged exposure to PDBu (15-min), FRET values were decreased to 0.6 $\pm$ 0.07 ($p < 0.01$; $n = 3$). Incubation with calyculin A did not influence this decrease (0.5 $\pm$ 0.08; $p < 0.01$; $n = 5$), but incubation with Gö6983 almost completely abolished the PKC-induced phosphorylation of the CKAR reporter (0.9 $\pm$ 0.05; $n = 3$). (*B*) $FRET_c$ values within the linearized plasma membrane of a representative COS1 cell expressing CKAR in the presence of calyculin A (*left panel*) or Gö6983 (*right panel*). Line colors correspond to the timepoints of the PDBu effect in the presence of calyculin A or Gö6983 in *A*. (*C*) Wavelet coefficient plots (values represented according to *color bar*) at control and after 1 and 15 min of PDBu exposure in the presence of calyculin A (*left panel*) or Gö6983 (*right panel*). All domains that were statistically significant at the 15 min PDBu effect, as revealed by the CWT, are indicated by brackets above and below the panels. In the presence of calyculin A, only one domain (marked with an asterisk) showed significant decrease in $FRET_c$ after 1-min exposure to PDBu, and no single domain showed a significant increase in $FRET_c$. In the presence of Gö6983, only one domain showed a significant change at 15 min of PDBu exposure, and no domains exhibited significant changes at 1 min.

then a wavelet transform could potentially be applied directly. However, in epifluorescent images, it is often problematic to manually define continuous ROI-containing pixels representing the plasma membrane. Redefining ROI_m based on a statistical analysis was an important step to avoid ambiguity of the traditional manual approach, and was crucial to our further analysis of signaling events. Some stimuli induce universal changes in FRET signals over a large part of the plasma membrane after prolonged exposure to an activator (such as PDBu). This property provides a method for identifying representative pixels from the plasma membrane (see Materials and Methods). By using only pixels showing statistically significant changes in $FRET_c$ values as a guide for defining a continuous plasma membrane, we decrease the bias introduced by visual inspection and eliminate neighbor pixels from plasma membrane pixels, which usually exhibit greater intensity (Fig. 2 *B*, *inset*).

We have applied the CWT to FRET signals in linearized ROI located within plasma membranes. This method of analysis is typically applied to time-series data. Unlike the traditional fast Fourier transform, the CWT co-localizes in both frequency (scale) and space (or time) domains. Although space-frequency localization can be achieved with a windowed Fourier transform, the efficient multiresolution representation of signals that contain transient properties, such as those observed in this study, is often better realized using wavelet analysis (Laine, 2000). For example, with a windowed Fourier transform, the width of the temporal or spatial window is prespecified and remains constant over the duration of the signal. However, a short window would be more desirable for assessing the high-frequency components of a signal, whereas a longer window or region would be needed for determining low-frequency information. Wavelet analysis represents a logical extension of the windowed Fourier technique, providing variable-sized windowing based on the scale of the wavelet basis function. Thus, wavelet analysis captures signal properties that may be missed by traditional techniques, such as fractal scaling (Arneodo et al., 1995). The wavelet decomposition consists of calculating a resemblance index (coefficients) between a signal and a wavelet basis function. Wavelet coefficient plots provide visualization of the changes in the heterogeneity of FRET signals at different timepoints and localize these changes within the plasma membrane ROI. For these signals and the

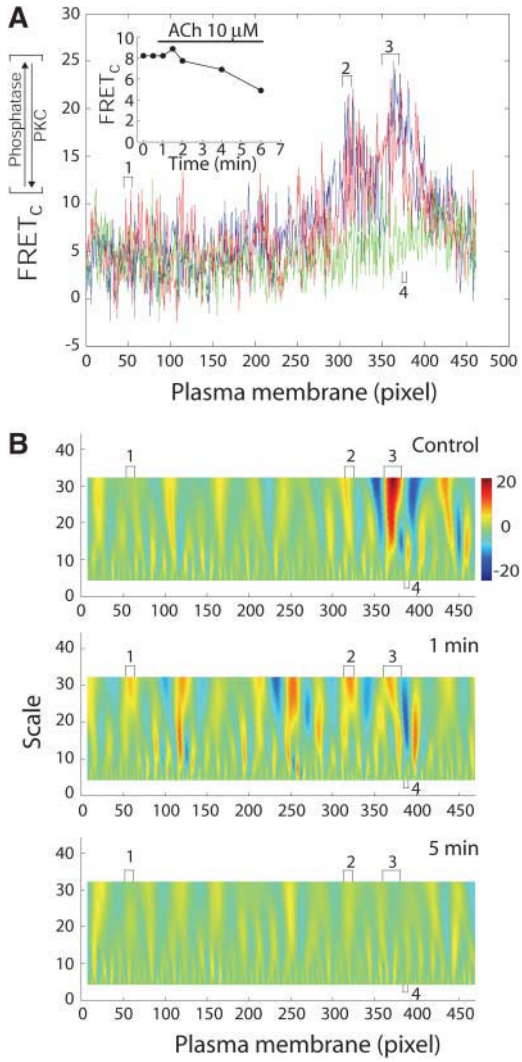

FIGURE 5 Activation of PKC by ACh (10 μM) in COS1 cells expressing CKAR and M1 muscarinic ACh receptor. (*A*) $FRET_c$ values in linearized plasma membrane ROI_s in control (*blue*) and after 1-min (*red*) and 5-min (*green*) application of ACh. Inset shows changes in $FRET_c$ averaged over the plasma membrane ROI_s. Decrease of $FRET_c$ values was due to phosphorylation of CKAR by PKC. (*B*) CWT analysis of $FRET_c$ in ROI_s using the db4 wavelet (values represented according to *color bar*). Standard deviations of wavelet coefficients were 2.65, 3.02, and 2.25 (scale 5) and 5.88, 5.44, and 2.36 (scale 32) at control, 1, and 15 min, respectively.

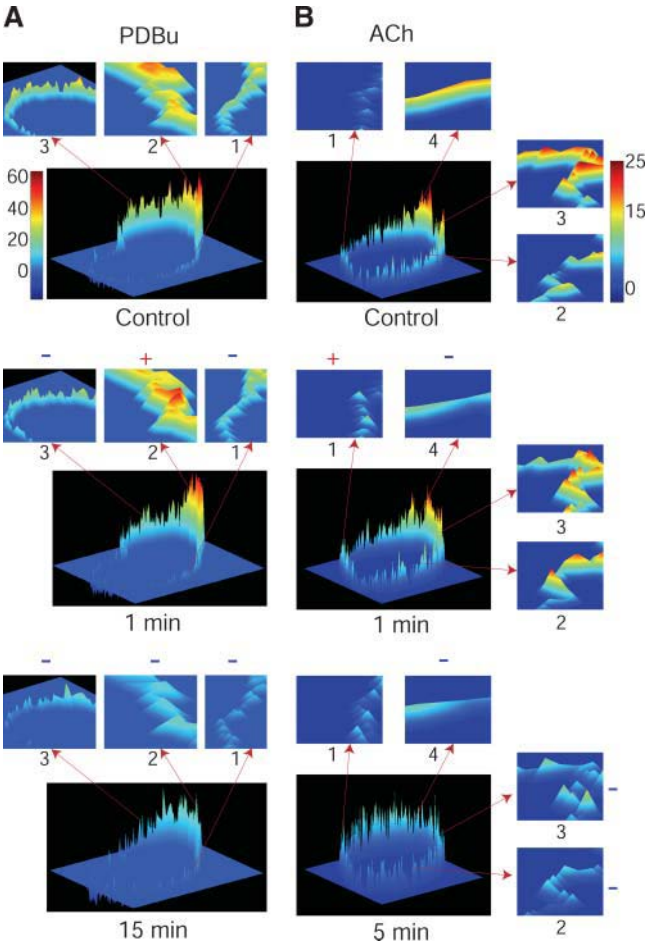

FIGURE 6 Three-dimensional representation of PKC activity in the statistically defined plasma membrane domains of COS1 cells expressing CKAR. (*A*) PKC activation by 200 nM PDBu. (*B*) PKC activation by 10 μM ACh. Color bars of $FRET_c$ are shown for both cells. Arrows point to the numbered domains that correspond to those marked by brackets in Figs. 2 and 5. Significant relative changes from the control images in the mean $FRET_c$ values in these domains (marked by *plus* or *minus symbols* above or on the *right side* of the images of microdomains) are reported in Table 1. Whereas all domains show decreased $FRET_c$ intensity at 15- (PDBu) and 5-min (ACh) timepoints, a local heterogeneity was observed in the 1-min ROI_s as several domains (1 and 3 in *A*, and 4 in *B*) responded oppositely to the average transient increases shown in Figs. 2 *B* and 5 *A (insets)*.

wavelets analyzed in this study (db4, db9, and Haar), our approach appears to be independent of the choice of the wavelet basis function (Fig. 2 *D*).

Image correlation microscopy/spectroscopy (ICM) is another image analysis technique that has shown considerable utility in characterizing the distributional heterogeneity in static images (Petersen et al., 1993). This analysis involves the calculation of an autocorrelation function, $G(\xi)$, such that

$$G(\xi) = \int_{-\infty}^{\infty} f(x)f(\xi + x)dx, \qquad (8)$$

where ξ represents a spatial shift. In other words, $G(\xi)$ is the correlation between a function, $f(x)$, and shifted versions of itself, as opposed to wavelet analysis, where a function is correlated with shifted and scaled versions of a wavelet basis function (Eq. 7). The autocorrelation function can be obtained by computing the inverse Fourier transform of the product of the Fourier transform of the signal and its complex conjugate (Press et al., 1992). A Gaussian function is then fitted to the normalized correlation data to estimate parameters that are used to calculate the density of fluorescent entities. Recently, ICM has been extended to include two dimensions and time-lapse sequences to map the molecular density, dynamics, and interactions of α5-integrin in

migrating cells (Wiseman et al., 2004). It would be of interest to compare the performance of ICM and wavelet-based analysis of FRET microscopy in future studies. Some immediate benefits of wavelet analysis include its multiresolution properties, the availability of commercially supported software, and its utilization in developing robust indices of spatial heterogeneity (Sharifi-Salamatian et al., 2004).

Both our wavelet-based approach and ICM are sensitive to the signal/noise ratio. Petersen et al. (1993) demonstrated that the density of fluorescent entities in an image calculated via ICM can result in erroneously high values in the presence of a low signal/noise ratio, and cautioned that careful controls are necessary in the presence of significant background fluorescence. To evaluate this issue with our wavelet-based method, five one-dimensional signals were generated that were 400 elements in length, where each value was randomly chosen between 0 and 1. We then added 0, 0.25, 0.5, 1, or 2 units to elements 197–203 in each signal, which were selected to represent a domain of interest. Wavelet analysis was conducted over 32 scales using the db4 wavelet basis function, and the difference matrices were computed with the zero-added signal serving as a control (see Wavelet Analysis in Materials and Methods). These matrices show that the domain was clearly identified for the 0.5-, 1-, and 2-unit added signals, but not the 0.25-unit added signal (see Fig. S1 in Supplementary Material). The 0.25-unit added signal was the only signal where the mean value of the domain (elements 197–203) did not significantly differ from that of the entire signal (Student's *t*-test; data not shown). Furthermore, as with the ICM method, a number of false-positives become evident as the signal/noise ratio decreases. However, our approach of conducting a statistical analysis of identified domains over time would serve to exclude the false-positives and retain domains with significantly changing corrected FRET intensities. The caveat of Petersen et al. (1993) is thus echoed here in that replications and/or measures over time with careful controls are required to ascertain the effects of noise.

In this study, the application of the CWT revealed a new aspect of PKC activation in real biological milieu. The transient increase in the FRET signal observed after 1 min of PDBu or ACh exposure (Figs. 2 *B* and 5 *A*) may be associated with a PKC-dependent activation of phosphatase, as it was hypothesized by Braz et al. (2004). In our control experiments, a pre-incubation of cells with a specific PKC inhibitor (Gö6983) or a phosphatase inhibitor (calyculin A) both completely eliminated this transient activation of phosphatase activity (Fig. 4 *A*). The lack of transient phosphatase activation has shifted the apparent balance in favor of PKC-induced phosphorylation and resulted in decrease of heterogeneity in plasma membrane domains. Note that overall, changes in $FRET_c$ over the plasma membrane were not significant, and only one domain showed a statistically significant decrease in $FRET_c$ values in the presence of calyculin A (Fig. 4 *C*, *left panel*), representing an increase in PKC-induced phosphorylation. The subsequent continuous stable decrease in $FRET_c$ reflects stimulation of PKC-dependent phosphorylation in membrane domains, which is sensitive to the PKC inhibitor Gö6983 (Fig. 4 *A* and Fig. 4 *B*, *right panel*) and highlights the complexity of the PKC signaling cascade.

In conclusion, we present a new strategy for the identification of functional signaling micro- and macrodomains of the plasma membrane by coupling FRET microscopy with wavelet analysis. This strategy includes: 1), redefining the plasma membrane into ROI_s based on statistical analysis; 2), applying the CWT to FRET values contained within the linearized ROI_s; and 3), identifying the heterogeneous regions from wavelet coefficient plots with consequent statistical analysis of corresponding regions in the plasma membrane. The implementation of this strategy facilitated the identification of plasma membrane domains of PKC signaling based on statistical analysis. These functional signaling domains putatively represent a dynamic balance of PKC phosphorylation and phosphatase activity. Furthermore, the balance in these domains is not necessarily represented by the average balance on the macrodomain scale, thereby offering a method to explore the importance of local heterogeneity in cell signaling in different experimental systems employing a variety of cell imaging techniques such as FRET, confocal, and fluorescence microscopy.

SUPPLEMENTARY MATERIAL

An online supplement to this article can be found by visiting BJ Online at http://www.biophysj.org.

The authors thank Dr. S. Sollott for critically reading the manuscript and Yasir Kazmi for help with calculations and preparation of figures. We also thank Drs. R.Y. Tsien and A.C. Newton for providing the CKAR-pcDNA3 constructs.

This study was supported by the Intramural Research Program of the National Institute on Aging, National Institutes of Health. None of the authors declare any competing financial interests that could be perceived as influencing this research.

REFERENCES

Aristizabal, F., and M. I. Glavinovic. 2003. Wavelet analysis of non-stationary fluctuations of Monte Carlo-simulated excitatory postsynaptic currents. *Biophys. J.* 85:2170–2185.

Arneodo, A., E. Bacry, P. V. Graves, and J. F. Muzy. 1995. Characterizing long-range correlations in DNA sequences from wavelet analysis. *Phys. Rev. Lett.* 74:3293–3296.

Braz, J. C., K. Gregory, A. Pathak, W. Zhao, B. Sahin, R. Klevitsky, T. F. Kimball, J. N. Lorenz, A. C. Nairn, S. B. Liggett, I. Bodi, S. Wang, A. Schwartz, E. G. Lakatta, A. A. DePaoli-Roach, J. Robbins, T. E. Hewett, J. A. Bibb, M. V. Westfall, E. G. Kranias, and J. D. Molkentin. 2004. PKC-α regulates cardiac contractility and propensity toward heart failure. *Nat. Med.* 10:248–254.

Haralick, R. M., K. Shanmugam, and I. Dinstein. 1973. Textural features for image classification. *IEEE Trans.* 3:610–621.

Kenworthy, A. K. 2001. Imaging protein-protein interactions using fluorescence resonance energy transfer microscopy. *Methods.* 24:289–296.

Kobrinsky, E., E. Schwartz, D. R. Abernethy, and N. M. Soldatov. 2003. Voltage-gated mobility of the Ca^{2+} channel cytoplasmic tails and its regulatory role. *J. Biol. Chem.* 278:5021–5028.

Kobrinsky, E., K. J. F. Kepplinger, A. Yu, J. B. Harry, H. Kahr, C. Romanin, D. R. Abernethy, and N. M. Soldatov. 2004. Voltage-gated rearrangements associated with differential β-subunit modulation of the L-type Ca^{2+} channel inactivation. *Biophys. J.* 87:844–857.

Laine, A. F. 2000. Wavelets in temporal and spatial processing of biomedical images. *Annu. Rev. Biomed. Eng.* 02:511–550.

Maxfield, F. R. 2002. Plasma membrane microdomains. *Curr. Opin. Cell Biol.* 14:483–487.

Misiti, M., Y. Misiti, G. Oppenheim, and J. M. Poggi. 2000. Wavelet Toolbox User's Guide. The MathWorks, Natick, MA.

Murata, S., P. Herman, and J. R. Lakowicz. 2001. Texture analysis of fluorescence lifetime images of nuclear DNA with effect of fluorescence resonance energy transfer. *Cytometry.* 43:94–100.

Murata, S., P. Herman, K. Mochizuki, T. Nakazawa, T. Kondo, N. Nakamura, J. R. Lakowicz, and R. Katoh. 2003. Spatial distribution analysis of AT- and GC-rich regions in nuclei using corrected fluorescence resonance energy transfer. *J. Histochem. Cytochem.* 51: 951–958.

Petersen, N. O., P. L. Hoddelius, P. W. Wiseman, O. Seger, and K. E. Magnusson. 1993. Quantitation of membrane receptor distributions by image correlation spectroscopy: concept and application. *Biophys. J.* 65:1135–1146.

Press, W. H., S. A. Teukolsky, W. T. Vetterling, and B. P. Flannery. 1992. Numerical Recipes in FORTRAN, 2nd Ed. Cambridge University Press, New York.

Sharifi-Salamatian, V., B. Pesquet-Popescu, J. Simony-Lafontaine, and J. P. Rigaut. 2004. Index for spatial heterogeneity in breast cancer. *J. Microsc.* 216:110–122.

Sharma, P., R. Varma, R. C. Sarasij, I. K. Gousset, G. Krishnamoorthy, M. Rao, and S. Mayor. 2004. Nanoscale organization of multiple GPI-anchored proteins in living cell membranes. *Cell.* 116:577–589.

Shirai, Y., and N. Saito. 2002. Activation mechanisms of protein kinase C: maturation, catalytic activation, and targeting. *J. Biochem.(Tokyo).* 132: 663–668.

Vermeer, J. E., E. B. Van Munster, N. O. Vischer, and T. W. Jr. Gadella. 2004. Probing plasma membrane microdomains in cowpea protoplasts using lipidated GFP-fusion proteins and multimode FRET microscopy. *J. Microsc.* 214:190–200.

Violin, J. D., J. Zhang, R. Y. Tsien, and A. C. Newton. 2003. A genetically encoded fluorescent reporter reveals oscillatory phosphorylation by protein kinase C. *J. Cell Biol.* 161:899–909.

Wallrabe, H., M. Elangovan, A. Burchard, A. Periasamy, and M. Barroso. 2003. Confocal FRET microscopy to measure clustering of ligand-receptor complexes in endocytic membranes. *Biophys. J.* 85:559–571.

Wiseman, P. W., C. M. Brown, D. J. Webb, B. Hebert, N. L. Johnson, J. A. Squier, M. H. Ellisman, and A. F. Horwitz. 2004. Spatial mapping of integrin interactions and dynamics during cell migration by image correlation microscopy. *J. Cell Sci.* 117:5521–5534.

Xia, Z., and Y. Liu. 2001. Reliable and global measurement of fluorescence resonance energy transfer using fluorescent microscopes. *Biophys. J.* 81: 2395–2402.

Zaccolo, M. 2004. Use of chimeric fluorescent proteins and fluorescence resonance energy transfer to monitor cellular responses. *Circ. Res.* 94: 866–873.

Zacharias, D. A., J. D. Violin, A. C. Newton, and R. Y. Tsien. 2002. Partitioning of lipid-modified monomeric GFPs into membrane microdomains of live cells. *Science.* 296:913–916.